ELSEVIER

Chemical Engineering Journal 141 (2008) 222–232

Chemical Engineering Journal

www.elsevier.com/locate/cej

Influence of salinity on bubble size distribution and gas–liquid mass transfer in airlift contactors

Duangkamol Ruen-ngam, Porntip Wongsuchoto, Apiradee Limpanuphap, Tawatchai Charinpanitkul, Prasert Pavasant *

Department of Chemical Engineering, Faculty of Engineering, Chulalongkorn University, Bangkok 10330, Thailand

Received 12 June 2007; received in revised form 21 December 2007; accepted 26 December 2007

Abstract

The investigation of the effect of salinity on the performance of airlift contactor was achieved using the 171 internal loop airlift with height of 1.2 m, and 0.137 m diameter. Various draft tubes with different diameter sizes were provided to vary the ratio between downcomer and riser cross-sectional areas (A_d/A_r) from 0.061 to 1.01. The superficial gas velocity (u_{sg}) was supplied in a range from 0.01 to 0.07 m/s and the salinity was adjusted from 0 to 45 ppt. The Sauter mean diameter of the bubble (d_{Bs}) appeared to be smaller in saline water than in fresh water. Bubble size was regulated by two factors. The first one was the hydrophilic repulsive force which inhibited bubble coalescence whereas the second was the Laplace pressure which controlled the coalescence and breakup of bubbles. The range of pressure difference, ΔP, acting on the bubble that promoted bubble coalescence was between 15 and 20 N/m^2 below which bubble coalescence was inhibited and above which bubble breakage prevailed. In saline water, d_{Bs} decreased with u_{sg}. This was caused by the collision and breakup of bubbles at high gas holdup which occurred at ΔP greater than 20 N/m^2. Axial variation in d_{Bs} was only observed at low u_{sg} (less than 0.04 m/s) where bubbles in the bottom section of the airlift were larger than those in the middle and top sections. It was anticipated that the middle and top sections exhibited higher turbulent conditions than the bottom section at this low aeration rate. The effect of draft tube size was quite important where the smallest draft tube (smallest downcomer area) best promoted the breakup of the bubbles with a relatively high ΔP of approximately 50–97 N/m^2. The effect of salinity on the overall volumetric mass transfer coefficient (k_La) was only apparent at high aeration rate where the fresh water provided a higher k_La than the saline water. In fact, the specific area (a) was high in the saline water systems, however, the mass transfer coefficient (k_L) was higher in the fresh water system than saline water. Finally, a general correlation for the estimation of k_L in the airlift system was proposed.

Keywords: Pressure difference; Bubble behavior; Mass transfer; Hydrodynamics

1. Introduction

An airlift system is an example of gas–liquid contacting devices for which its application in biotechnology area has grown significantly in recent years [1–4]. Examples include the cultivation of fresh water single cell algae *Haematococcus pluvialis* as proposed by Kaewpintong et al. [5] and the high productivity of the sea water diatom *Chaetoceros calcitrans* in airlift photobioreactors as proposed by Krichnavaruk et al. [6,7]. One of the most significant parameters in the design of such airlift systems is the overall volumetric mass transfer coefficient which is commonly employed to demonstrate the efficiency of oxygen transfer from gas to liquid. This quantity depends on the system geometry and liquid properties which are related to several other parameters. Principally, this parameter is constituted of the mass transfer coefficient (k_L) and the specific interfacial area (a_L) which then depends on the flow regimes, hydrodynamics and bubble characteristics in the system. Information regarding bubble size distribution is often useful as it determines the level of interfacial mass transfer and other hydrodynamic behavior of the systems. However, the availability of such information is quite sparse. Literature reported that bubble breakage was a predominant factor in the gas–liquid contacting devices particularly at high gas throughputs [8–11]. Hence, the systems at high aeration rate are typically operated with smaller bubble size range which enhances gas holdup and consequently gas–liquid mass transfer. Bubble breakage was also found to take place along the height of the column due to an increasing interaction between

* Corresponding author. Tel.: +66 2 218 6870; fax: +66 2 218 6877.
E-mail address: prasert.p@chula.ac.th (P. Pavasant).

1385-8947/$ – see front matter © 2008 Elsevier B.V. All rights reserved.
doi:10.1016/j.cej.2007.12.024

Nomenclature

a	specific interfacial area based on liquid volume (m^2/m^3)
A	cross-sectional area (m^2)
c	dissolved oxygen concentration (mg/l)
c^*	saturated dissolved oxygen concentration concentration (mg/l)
c_L	oxygen concentration in liquid phase (mg/l)
c_o	initial dissolved oxygen concentration (mg/l)
$d_{B,i}$	sphere bubble diameter with the same volume as ellipsoidal bubble (mm)
d_{Bs}	Sauter mean diameter (mm)
D_l	diffusivity (m^2/s)
D_i	inside diameter of draft tube (cm)
D_{io}	outer diameter of draft tube (cm)
h_i	video level (cm)
h	height of defined liquid level in the column (cm)
H_L	unaerated liquid height (m)
H_D	aerated liquid heights (m)
g	gravitational acceleration (m/s^2)
k_g	overall mass transfer coefficient (m/s)
k_L	overall mass transfer coefficient (m/s)
k_La	overall volumetric mass transfer coefficient (l/s)
n_i	occurrence frequency number
p	major axes of bubble images
ΔP	pressure difference acting on bubbles (N/m^2)
ΔP_m	pressure difference between the two measuring ports (N/m^2)
q	minor axes of bubble images
t	time (s)
u_{sg}	superficial gas velocity (m/s)
u_α	terminal rise velocity of bubble (m/s)

Greek symbols

δ	film thickness (cm)
ε_d	downcomer gas holdup
ε_o	overall gas holdup
ε_r	riser gas holdup
μ	viscosity (kg/m s)
ρ	density (kg/m^3)
σ	surface tension (N/m)

bubbles as they traveled up the top of the column [2]. Wongsuchoto et al. [4] reported that bubble breakage occurred more at the top part resulting in smaller bubble size to be smaller than that at the lower part. Electrolyte solutions such as sea water were reported to provide a higher k_La than that in fresh water as the bubble size in such systems was relatively small. On the other hand, systems with higher viscosity such as CMC (carboxymethyl cellulose) exhibited a lower k_La than those running with lower viscosity mediums [12,13]. The presence of antifoam promoted bubble coalescence and therefore reduced k_La [13,14]. Apart from the liquid properties, the reactor design parameters such as the height of the column and the ratio between riser and downcomer cross-sectional area (A_d/A_r) could also affect the flow pattern and bubble size distribution in the airlift system.

The gas–liquid mass transfer is commonly considered as a function of bubble sizes, and is explicitly described in several empirical correlations such as Frossling's equation and Higbie's theory for bubble columns [15]. Although the application of airlift could be in mediums with various properties, most investigations on bubble size distribution are often confined to the system operated with water–air as liquid and gas phases, respectively. Salinity is known to alter the properties of water, for instance, it decreases the surface tension of the solution, and this could significantly affect the bubble size distribution. This, in turn, has notable influence on the gas–liquid mass transfer. This work therefore focused on the quantitative analysis of the influence of salinity on the hydrodynamics and mass transfer behavior of the annulus sparged internal loop airlift contactor.

2. Experimental

2.1. Apparatus

Experiments were carried out in an acrylic transparent airlift contactor as detailed in Fig. 1. The column was 1.2 m in height with an inside diameter of 0.137 m. The column was equipped with pressure taps along the contactor height for the measurement of pressure drop, ΔP, which was used to determine riser gas holdup, $\varepsilon_{g,r}$. A 1 m draft tube height was installed centrally in the column with a bottom clearance of 5 cm for liquid circulation. The ratio between cross-sectional areas of downcomer and riser (A_d/A_r) was altered by changing the draft tube diameter as detailed in Table 1. Saline water was added into the column until the anaerated liquid height was 3 cm above the draft tube. The aeration was accomplished through a perforated ring sparger with 30 holes (1 mm in diameter) provided at the base of the annulus section. The sparger was made from PVC tubing with 0.8 cm diameter. Air flow rate was controlled by a calibrated rotameter to give a range of superficial gas velocities, u_{sg}, from 0.01 to 0.07 m/s.

Table 1 summarizes detail of the operation of this system. The salinity was measured by OPTIK Handheld Refractometer and was controlled at 15, 30, and 45 ppt. The density of the solution was measured by pycnometer (UL/Y ADAPTER, MIDDLE BORO, MA 02346, U.S.A., Brook field ENGINEERING LABS INC.) at 100 rpm, 26.5 °C, and the surface tension was measured with KRUSS K10T (Du Noüy Ring). These properties were summarized in Table 2.

Table 1
Dimensions of draft tubes

Draft tube	Symbol	D_i (cm)	D_{io} (cm)	A_d/A_r (−)
1	ALC1	3.4	4	0.067
2	ALC2	7.4	8	0.443
3	ALC3	8.4	9	0.661
4	ALC4	9.4	10	1.008

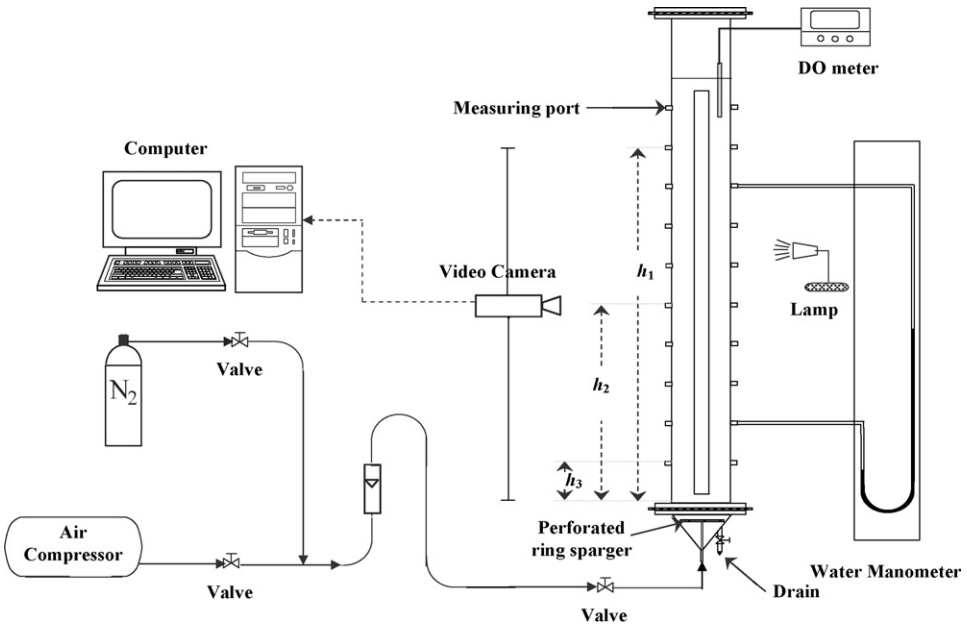

Fig. 1. Schematic diagram of concentric internal loop airlift contactor employed in this work.

Table 2
Liquid properties

Liquid phase	Surface tension (N/m)	Viscosity (kg/m s)	Density (kg/m^3)
Tap water	72.6×10^{-3}	1.28×10^{-3}	0.996×10^3
Sea water at 15 ppt	73.1×10^{-3}	1.44×10^{-3}	1.005×10^3
Sea water at 30 ppt	73.7×10^{-3}	1.47×10^{-3}	1.016×10^3
Sea water at 45 ppt	73.9×10^{-3}	1.49×10^{-3}	1.027×10^3

Table 3
Locations of digital video camera for bubble size measurement

Section	Height from the bottom end of the draft tube (h_i) (cm)
Top section (h_1)	90
Middle section (h_2)	50
Bottom section (h_3)	10

2.2. Bubble size distribution measurement

The bubble size measurement was performed in riser section using a photographic technique. More than 200 bubbles were photographed using a digital camcorder (Panasonic® NV-GS75) at three different heights (h_i): 10 cm (bottom section), 50 cm (middle section) and 90 cm (top section) from the base of the draft tube as illustrated in Fig. 1 and Table 3. The operating conditions for all ALC systems are given in Table 4. The correction to real size was based on the scale attached to the draft tube with the same focal distance as the measured bubbles. The focus was adjusted on the scale and only the well-focalized bubbles were measured [4]. For ellipsoidal bubbles, the major and minor axes of bubble images were measured. The equivalent size of the bubble (d_B), representing the diameter of a sphere whose volume was equal to that of the bubble, is calculated using Eq. (1) [16,17].

$$d_B = (p^2 q)^{1/3} \tag{1}$$

2.3. Determination of hydrodynamic and mass transfer behavior of airlift contactors

The overall gas holdup, $\varepsilon_{g,o}$, was determined by the volume expansion method where:

$$\varepsilon_{g,o} = \frac{H_D - H_L}{H_D} \tag{2}$$

Table 4
Operating conditions for each ALC system

ALCs	Superficial gas velocity (m/s)					
	①	②	③	④	⑤	⑥
ALC1	0.008	0.012	0.018	0.022	0.030	0.035
ALC2	0.011	0.016	0.025	0.031	0.041	0.048
ALC3	0.013	0.019	0.029	0.036	0.048	0.056
ALC4	0.016	0.023	0.035	0.044	0.058	0.068
Symbol	·····	———	– – – –	-------	———	–·–·–

The riser gas holdup, $\varepsilon_{g,r}$, was estimated by measuring the pressure difference (ΔP_m) between two pressure taps located along the height of the column (Δh) where:

$$\varepsilon_{g,r} = 1 - \frac{\Delta P_m}{\rho_l g \Delta h} \quad (3)$$

It was assumed that gas holdup in the top section was approximately equal to that in the riser and therefore the downcomer gas holdup, $\varepsilon_{g,d}$, could be computed from:

$$\varepsilon_{g,d} = \frac{\varepsilon_{g,o} H_D (A_d + A_r) + (H_{df} A_d - H_D (A_d + A_r)) \varepsilon_{g,r}}{H_{df} A_d} \quad (4)$$

Liquid velocities both in riser and downcomer were measured using the color tracer technique. The pressure taps were employed as injection points of the color tracer and the recorded time of color tracer between the two points in the contactor was measured for the calculation of liquid velocity.

The overall volumetric mass transfer coefficient ($k_L a$) was determined by the dynamic method [18–20]. A dissolved oxygen meter (Jenway 9300) was used to record the changes in oxygen concentration with time in the ALC. The system was initially freed of O_2 by bubbling N_2 through the liquid for approx. 10 min. The calculation of $k_L a$ follows Eq. (5):

$$\ln \frac{(c* - c_\circ)}{(c* - c_L)} = k_L a t \quad (5)$$

3. Results and discussion

3.1. Local bubble size distribution in airlift systems

Fig. 2 illustrates examples of the bubble size distribution curves obtained from the various sections of the ALC system operated with saline water at 30 ppt and with $A_d/A_r = 0.661$. As a general trend, bubble size was quite large, in the range of 6.0–8.2 mm, at low superficial velocity. At higher gas throughput, bubbles became smaller in size and the distribution of bubble size became bimodal where there were two main bubble sizes present at the same time (2 and 6.5 mm). At high gas throughput, bubble size became small and the distribution illustrated that there was only one main bubble size in the system at this condition (2 mm). Bubble size did not seem to be smaller when the superficial velocity became higher than 0.036 m/s. This finding was for the system operated with water at salinity of 30 ppt, and it agreed well with the report by Wongsuchoto et al. [4] who carried out the experiment in fresh water systems that, at adequately high aeration, bubble no longer changed its size distribution ($u_{sg} > 0.05$ m/s). The difference was that the airlift operated with saline solution had smaller bubble sizes than those with fresh water.

3.2. Axial bubble size distribution in airlift contactors

The axial bubble size distribution was obtained by taking photographs of bubbles in the airlift at different heights. Bubble distribution frequency was then formulated for each sampling point, and the results are given in Fig. 2. In the top and middle

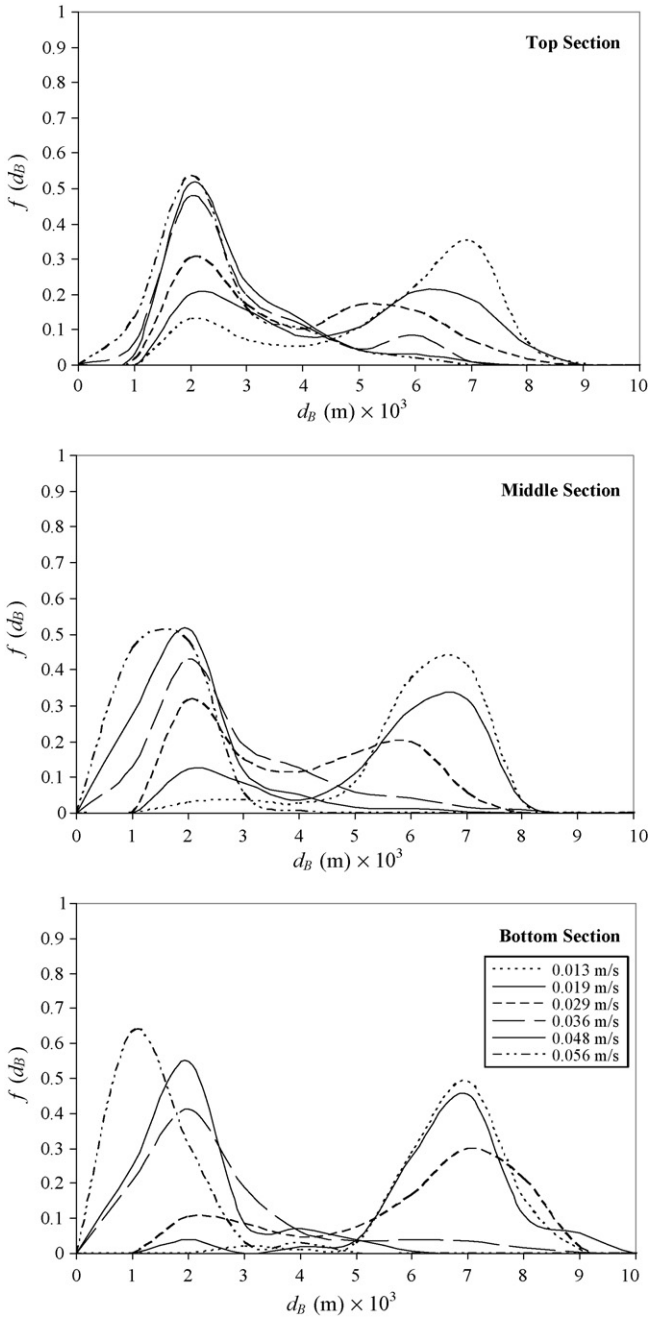

Fig. 2. Frequency distribution of bubble sizes at various superficial gas velocities in ALC with $A_d/A_r = 0.661$ (salinity = 30 ppt).

sections, the distribution changed from uni-modal to multi-modal curve at $u_{sg} \approx 0.019$ m/s whereas the bottom section saw this change at $u_{sg} \approx 0.029$ m/s. The breakage of the bubbles at high gas throughput was caused by higher amount of energy dissipation and turbulent which promoted more interaction between bubbles. The results suggested, therefore, that there was a higher level of turbulence in the top and middle sections than that in the bottom. Fig. 3 illustrates the mean values of the bubble sizes with the highest occurrence frequencies (Fig. 3(a)) compared with the average, Sauter mean diameter of bubbles (Fig. 3(b)) in the three sections in the airlift system with A_d/A_r of 0.661. This revealed that bubble size in the bottom section was slightly larger

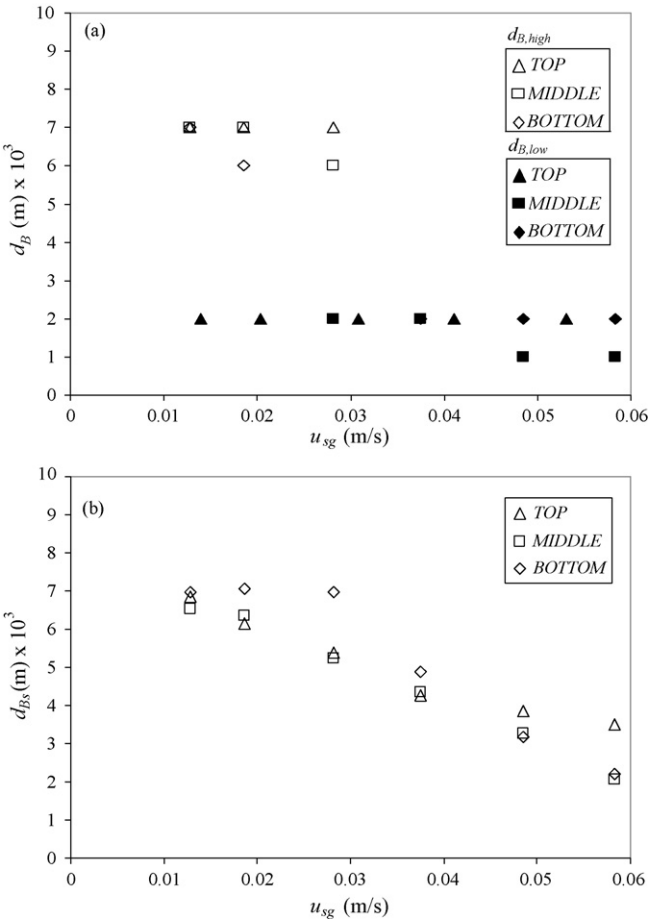

Fig. 3. Axial variation in bubble size in ALC with $A_d/A_r = 0.661$ (salinity = 30 ppt): (a) the average high bubble size ($d_{b,high}$) and average low bubble size ($d_{b,low}$), and (b) Sauter mean diameter.

than in those in the other sections, particularly at a lower range of u_{sg} (<0.04 m/s) examined in this work. At a higher u_{sg} range, the effect of column height on the bubble size was not obvious and the sizes of bubbles were approximately the same throughout the length of the airlift. The same finding was found for the system running with tap water as described in Wongsuchoto et al. [4].

3.3. Effect of the ratio between downcomer and riser cross-sectional areas on bubble size

To investigate the effect of the ratio between the downcomer and riser cross-sectional areas (A_d/A_r), the experiment was conducted in the airlift contactors running with sea water at 30 ppt with four different draft tube sizes as detailed in Table 1 and the average bubble sizes are shown in Fig. 4. At a low range of u_{sg} (<0.015 m/s), no significant differences in bubble size were observed in all systems. At u_{sg} greater than 0.015 m/s, the differentiation of the bubble sizes in the systems with different draft tube sizes became more obvious, i.e. the bubble size was larger in the system with larger draft tube size (d_{Bs}, ALC4 > 3 > 2 > 1). In other words, the bubble size was larger in the system with smaller riser cross-sectional area. It was possible that turbulence in the system with smaller riser was stronger than those with larger riser, and increasing the chance of bubbles being coalesced. Fig. 4 also illustrates that the effect of A_d/A_r on bubble size was more obvious at the bottom section, and not as much in the middle and top sections. As stated earlier, the level of turbulence in the middle and top sections of the airlift was believed to be stronger than that in the bottom section. However, bubble sizes in this top section were not significantly regulated by A_d/A_r suggesting that, within the range of aeration employed in this work, similar level of turbulent intensity was resulted. On the other hand, the bottom section in the airlift with different A_d/A_r might be exposed to noticeable levels of turbulence inten-

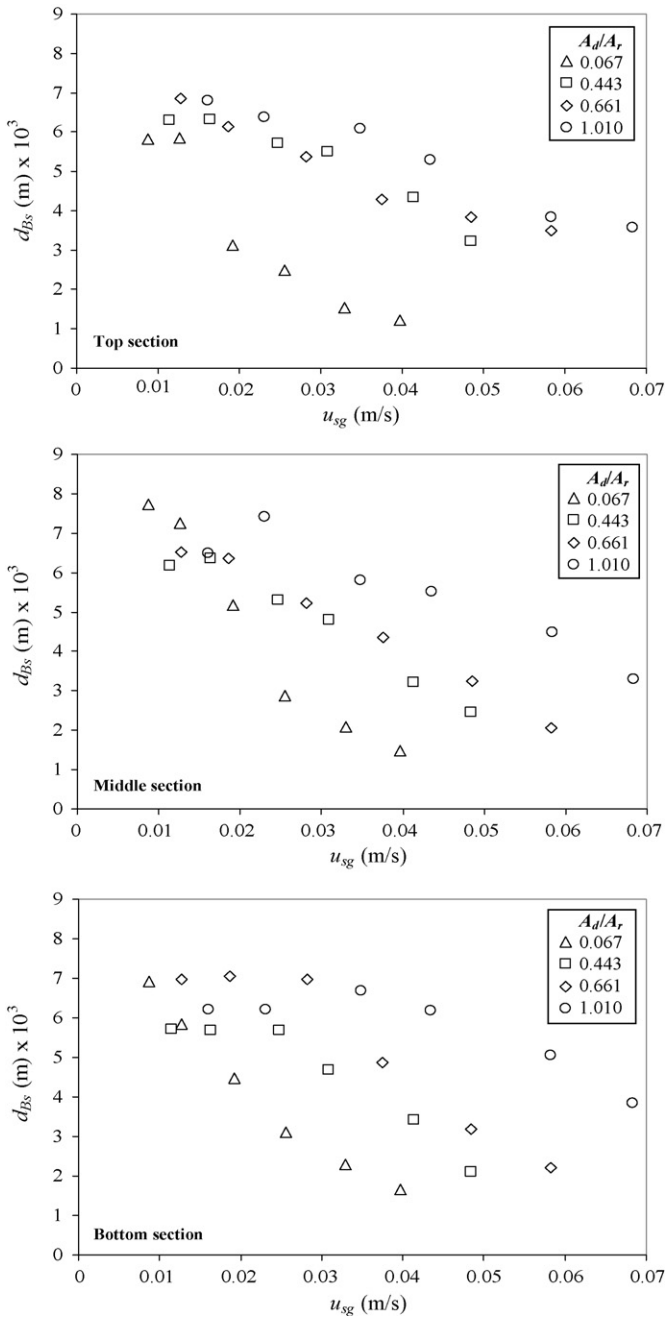

Fig. 4. Bubble sizes in ALC with different downcomer to riser cross-sectional area ratios (salinity = 30 ppt).

sities. This therefore resulted in a distinguishable bubble sizes as observed in Fig. 4.

3.4. Effect of salinity on average bubble size

Fig. 5(a–b) displays the relationship between bubble sizes in the ALC operated with saline water at different salinity levels. This figure illustrates that, at low range of u_{sg} (<0.02 m/s), the effect of salinity on bubble size was not obvious and bubble sizes were in the range of 6.0–7.5 mm in all ALC systems. At higher u_{sg}, the effect of salinity on bubble size became more apparent where the bubble size appeared to be smaller in the saline solution than that in fresh water. This was in contrast with the fact that saline solution possesses stronger surface tension and viscosity than water and the bubble size in such solution should be larger than that in water. However, in this case, the effect of electrolyte on viscosity (Marangoni effect) was reported not to be adequate to regulate the bubble size [21,22], and therefore the effects of salinity on bubble size were mainly due to its ionic properties. This finding was in good agreement with several past reports which stated that electrolyte solutions inhibited bubble coalescence and retarded bubble riser velocity which then reduced the bubble size [20,22–26]. It should be noted that types and concentration of electrolytes can impose different effects on bubble coalescence, for instance, Lessard and Zieminiski [20] ordered the coalescence efficiency in various electrolytes as follows: $MgSO_4 < MgCl_2 < CaCl_2 < Na_2SO_4 < LiCl < NaCl < NaBr < KCl$.

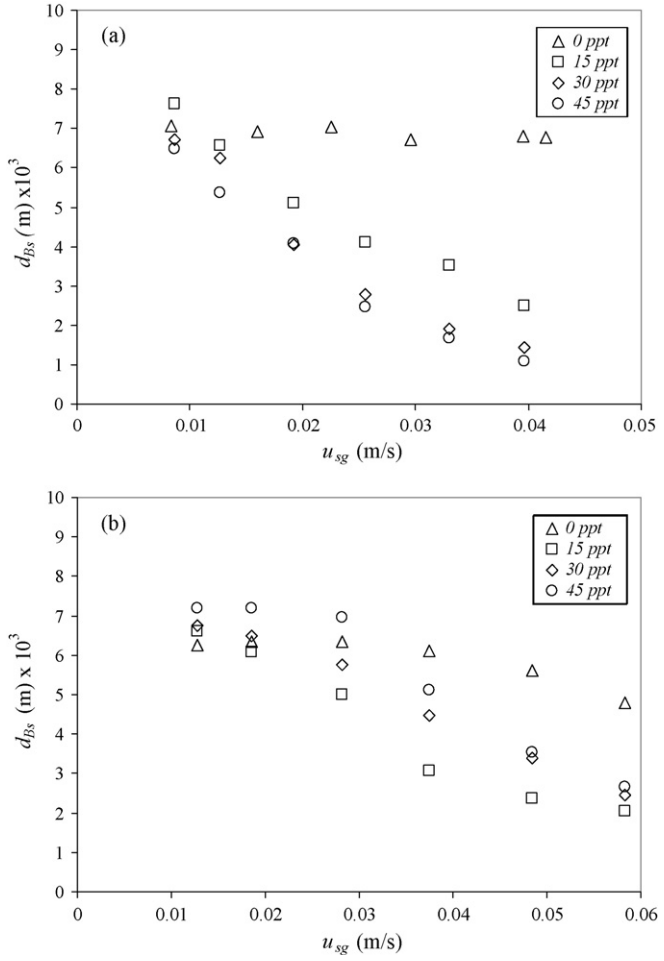

Fig. 5. Bubble sizes in ALC: (a) $A_d/A_r = 0.067$ and (b) $A_d/A_r = 0.661$.

Fundamentally, there are two types of forces or pressures dealing with the coalescence or breakup of the bubbles. The first one is the Laplace pressure which promotes bubble coalescence caused by the drainage of the liquid film located in between the two adjacent bubbles. This pressure depends on the reciprocal of the bubble diameter. However, if the Laplace pressure is too strong, bubbles coalesce very rapidly and this reduces the stability of the bubbles. Therefore, at this condition, bubble breakage dominates in the system. The other type of force is repulsive force. Electrolytes such as salt increased the repulsive hydration force by enhancing water structure due to hydrogen bond at the interface leading to a more stable bubble than that in the fresh water system. This formation of repulsive force balances the Laplace pressure, inhibiting bubble coalescence. The two forces can be written in a mathematical form as follows [27]:

$$\Delta P = \frac{\sigma}{r_p} - \Pi \tag{6}$$

when σ is surface tension, r_p is radius of intersection of three films called the Plateau border channel and the ratio between the surface tension and radius of intersection or (σ/r_p) is equal to Laplace pressure. Π is the repulsive pressure or disjoining pressure which is the summation of various forces between ions interaction at the gas and liquid interface according to Eq. (7).

$$\Pi = \Pi_{vdw} + \Pi_{DL} + \Pi_{hyd} \tag{7}$$

where Π_{vdw} is attractive van der Waals force, Π_{DL} is the dielectric double layer force or repulsive force and Π_{hyd} is short-range repulsive or hydration force. An attractive van der Waals force (Π_{vdw}) is a weak attraction force and caused from the polarization of molecules into dipoles, and can be expressed mathematically as in Eq. (8). A dielectric double layer (Π_{DL}) is the repulsive force caused from confinement of the ion charge at gas–liquid interface. A hydration force was short-range repulsive force (Π_{hyd}) resulting from the formation of the water molecules near charged surfaces as in Eq. (9),

$$\Pi_{vdw} = \frac{-A}{6\pi h^3} \tag{8}$$

$$\Pi_{hyd} = \left(\frac{W}{\lambda}\right) \exp(-h/\lambda) \tag{9}$$

where A is the Hamaker constant which is equal to 10^{-20} J, h the film rapture thickness, λ the decay length of the hydration interaction, mostly takes the value of about 8.5 nm, and W the pre-exponential constant ≈6 mN/m^2 [27]. The film rapture thickness or h was reported to be a function of salinity by Cain and Lee [28] which were equal to 114.7, 106.8, 98.8, and 90.9 for the water with salinity levels of 0, 15, 30, and 45 ppt, respectively. In the same work [28], it was reported that the dielectric double layer force (Π_{DL}) was negligible compared with the hydration force and should be omitted from the calculation. Moreover, van der Waals attraction was generally reported to be relatively

Table 5
Estimates of disjoining pressures (Π) at different salinity levels

Salinity (ppt)	h[a] (nm)	van der Waals attraction (N/m^2)	Electrostatic repulsion (N/m^2)	Hydration repulsion (N/m^2)	Total pressure (Π) (N/m^2)
0	114.7	−0.35	0	0.97	0.62
15	106.8	−0.44	0	2.47	2.03
30	98.8	−0.55	0	6.29	5.74
45	90.9	−0.71	0	16.01	15.30

[a] [28].

small and was also negligible compared with the hydration force [21,22]. Therefore, Eq. (6) is reduced to

$$\Delta P = \frac{\sigma}{r_p} - \Pi_{hyd} \quad (10)$$

The pressure difference, ΔP, in Eq. (10) was important in controlling the level of bubble coalescence or bubble breakage in the system. ΔP is low for the condition with inhibiting bubble coalescence, and high for the bubble coalescence promoting conditions. Nevertheless, as mentioned above, a much higher ΔP would result in a breakup of bubbles [29]. A summary of these forces acting on the bubbles in the airlift systems is given in Table 5.

Let us define the parameter ΔP_C which is the level of ΔP below which the inhibition of bubble coalescence occurred, and above which bubble breakage prevailed. Therefore, the bubble had its greatest size at ΔP_C. Fig. 6 shows the summary of the various forces acting in the various saline solutions. As stated earlier, the bubble size in the water system was the largest and under this condition, ΔP in water was approx. 20 N/m^2 for the whole range of u_{sg} employed in this work as detailed in Table 6. This was due to the absence of repulsive force to balance the Laplace pressure. With the presence of salinity, the repulsive force became stronger. However, this repulsive force was not strong enough to bring ΔP down. In contrast, the Laplace pressure in the presence of salinity seemed to be quite large which could be the result from the increasing surface tension. This resulted in ΔP having a value greater than 20 N/m^2. Therefore, bubbles tended to break in such condition.

In the airlift with A_d/A_r of 0.067 running with 45 ppt salinity, ΔP was about 43–121 N/m^2 at $u_{sg} > 0.02$ m/s and therefore bubble breakup was expected. The bubble size in this case was quite small, at 0.001–0.002 m (see Fig. 5(a)). Fig. 5(b) illustrates that when the A_d/A_r was altered (from 0.067 to 0.661), the condition in the system changed, and despite using the same level of u_{sg}, the system running with 45 ppt salinity had ΔP of 5–25 N/m^2 which prevented bubble breakup, therefore accommodating larger bubbles (0.005–0.006 m) than those in the airlift with lower A_d/A_r.

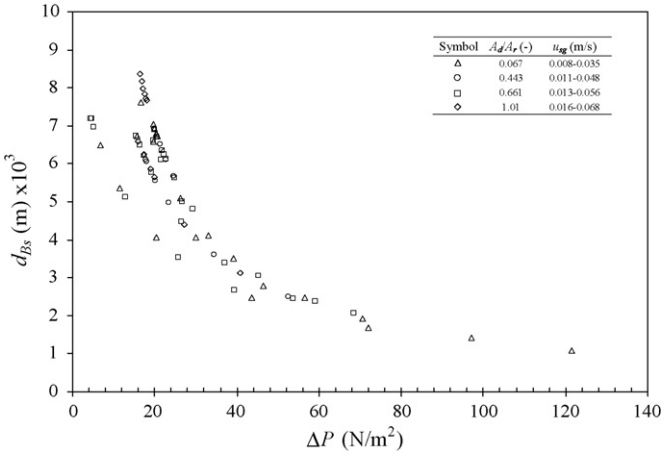

Fig. 6. Relationship between bubble size and ΔP.

Fig. 6 illustrates the relationship between pressure driving forces and the average bubble size in all airlift systems employed in this work. It seemed that ΔP that gave the largest bubble size (ΔP_C) was in the range from 15 to 20 N/m^2.

3.5. Effect of superficial velocity

Fig. 5(a–b) demonstrates that Sauter mean diameter of the bubbles decreased with superficial gas velocity at all salinity levels. This finding agreed well with the reported data in the airlift systems operated with various types of liquid [2–4,30]. The bubble sizes were regulated by the level of pressure difference

Table 6
Estimates of pressure driving forces for average bubble size in different salinity levels in ALC with $A_d/A_r = 0.067$

Salinity (ppt)	u_{sg} (m/s)	ΔP (N/m^2)	d_{Bs} (m) × 10^3
0	0.008	19.61	7.05
	0.012	19.97	6.94
	0.018	19.62	7.05
	0.022	20.62	6.72
	0.030	20.36	6.81
	0.035	20.45	6.78
15	0.008	16.69	7.63
	0.012	19.76	6.58
	0.018	26.24	5.09
	0.022	33.10	4.11
	0.030	39.15	3.51
	0.035	56.48	2.48
30	0.008	15.61	6.73
	0.012	17.29	6.25
	0.018	30.00	4.06
	0.022	46.38	2.80
	0.030	70.66	1.92
	0.035	97.02	1.43
45	0.008	6.79	6.48
	0.012	11.54	5.37
	0.018	20.30	4.07
	0.022	43.73	2.47
	0.030	71.90	1.68
	0.035	121.4	1.08

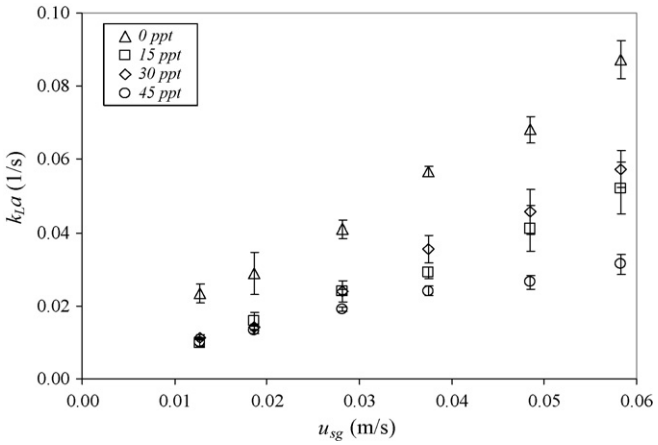

Fig. 7. Overall volumetric mass transfer coefficient (ALC with $A_d/A_r = 0.661$).

in the airlift system as described earlier. At low range of gas flow rate (<0.02 m/s) as shown in Fig. 5(a), the pressure difference was in the range of 15–20 N/m^2, and this enhanced bubble size. At a higher range of superficial gas velocity (>0.02 m/s), ΔP was higher than 20 N/m^2 which promoted the breakup of the bubbles. In addition, at this high gas throughput conditions, the airlift contained a relatively high gas holdup which also enhanced the chance of bubbles collision and breaking up.

3.6. Overall volumetric mass transfer coefficient (k_La) in the airlift systems operating with sea water

The overall volumetric mass transfer coefficient (k_La) was calculated from Eq. (5). The change in k_La with u_{sg} and salinity level is illustrated in Fig. 7 which shows that k_La increased with superficial gas velocity but decreased with an increase in salinity. Salinity seemed to have adverse effects on k_La and the system with fresh water always imposed a higher k_La than those running with sea water. In addition, the effect of salinity on k_La was quite complicated. At low range of u_{sg} (<0.03 m/s), the effect of salinity did not seem to be significant, however, the effect became more pronounced at high aeration rate ($u_{sg} > 0.03$ m/s) and k_La was the highest at 30 ppt followed by those at 15 and 45 ppt, respectively.

This k_La quantity composed two main parameters, i.e. "k_L" or overall mass transfer coefficient, and "a" or specific interfacial area. Generally k_L was reported to be a function of turbulence, liquid properties and bubble size. The specific interfacial area (a) can be estimated using Eq. (11):

$$a = \frac{6\varepsilon_g}{d_{Bs}(1-\varepsilon_g)} \tag{11}$$

where $\varepsilon_{g,r}$ is the riser gas holdup and d_{Bs} Sauter mean diameter which is defined as:

$$d_{Bs} = \frac{\sum n_i d_{B,i}^3}{\sum n_i d_{B,i}^2} \tag{12}$$

where n_i is the occurrence frequency number of the sphere bubbles diameter, $d_{B,i}$. The two parameters significant for the determination of the specific mass transfer area were average

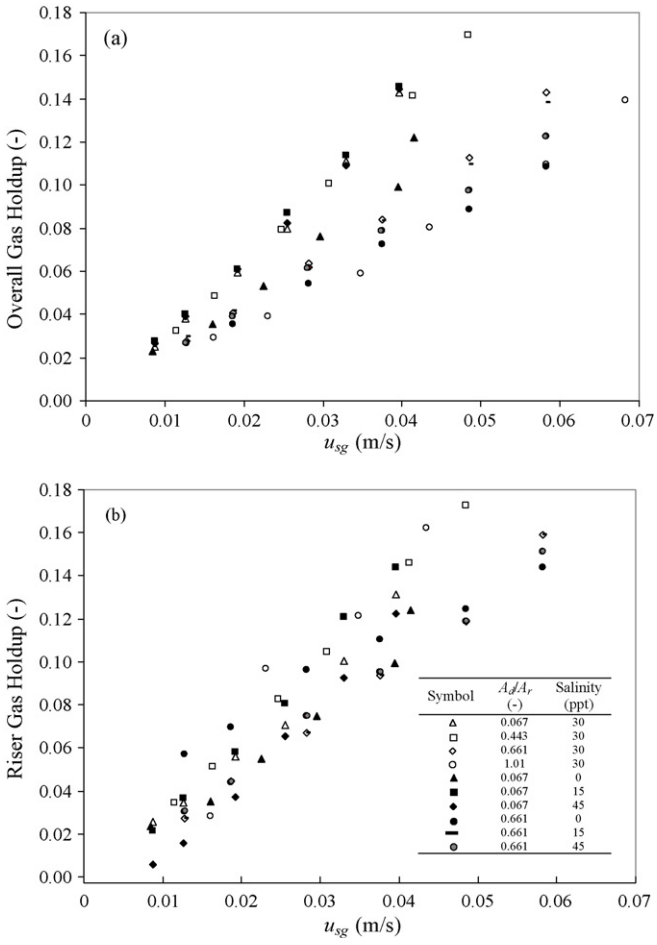

Fig. 8. Effects of superficial gas velocity, u_{sg}, on gas holdups.

bubble size (Fig. 5(b)) and gas holdup. Fig. 8 illustrates that the effect of salinity on gas holdups in the system was only marginal and the specific area should only vary with bubble size. As discussed earlier, the bubble size in sea water was smaller than that in fresh water and became smaller with an increase in superficial gas velocity. Therefore, the specific interfacial areas obtained in the systems at all salinity levels were higher than that in the fresh water system.

It was primarily assumed that the gas holdup was uniform throughout, both in axial and radial directions. The estimates of specific interfacial area (a) in the airlift system with $A_d/A_r = 0.661$ at various salinities is displayed in Fig. 9. This finding revealed that effect of salinity on specific area was only marginal at low range of superficial gas velocity ($u_{sg} < 0.028$ m/s), and became more significant at higher u_{sg}. The largest gas–liquid surface area was obtained from the airlift operating with saline water at 15 ppt, followed by those at 30 and 45 ppt. This corresponded well with the information on the effect of salinity on bubble size in Fig. 5(b).

Now that the information on k_La and a became known, the overall mass transfer coefficient or k_L could simply be calculated by dividing k_La with a and the results are given in Fig. 10. The results revealed that k_L only became significantly different at high u_{sg}. The pure water system provides the highest level of

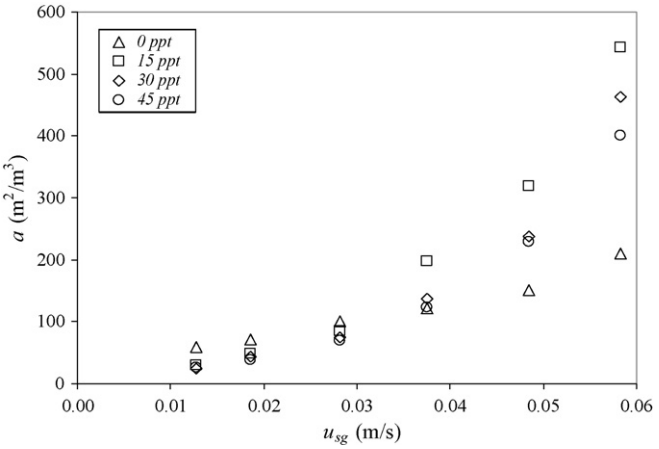

Fig. 9. Specific interfacial area in ALC ($A_d/A_r = 0.661$).

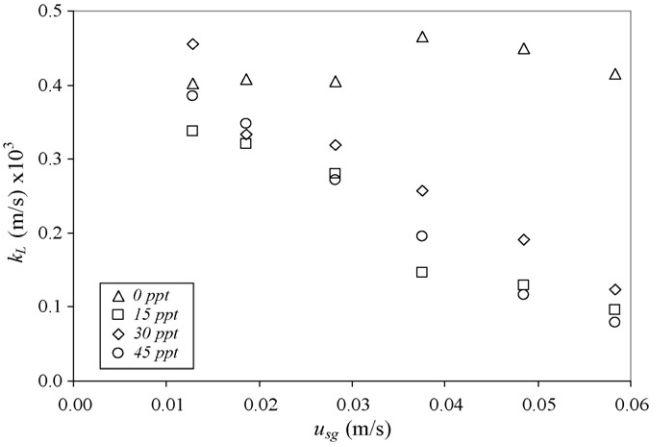

Fig. 10. Effects of superficial gas velocity, u_{sg}, on overall specific mass transfer coefficient, k_L, in ALC ($A_d/A_r = 0.661$).

k_L. Among the saline solutions, k_L was highest in the system with salinity of 30 ppt, followed by that with 45 ppt and 15 ppt, respectively. The reason fore this variation still could not be retrieved from this experiment. However, it was observed that the trend in k_La followed that of k_L quite closely, i.e. the highest was in pure water system, followed by those in saline concentrations of 30, 45 and 15 ppt, respectively.

3.7. Estimate of k_La

The mass transfer rate for the entire contactor was proposed in terms of the overall volumetric mass transfer coefficient $(k_La)_T$ and could be calculated from sum of the mass transfer rates in riser and downcomer section as follows:

$$(k_La)_T = \frac{(k_La)_r V_{L,r} + (k_La)_d V_{L,d}}{V_{L,T}} \quad (13)$$

where $V_{L,r}$ is the volume of liquid in riser, $V_{L,d}$ the volume of liquid in downcomer and $V_{L,T}$ the volume of total liquid. $(k_La_L)_r$ and $(k_La_L)_d$ were then obtained from multiplied $k_{L,r}$ by $a_{L,r}$ and $k_{L,d}$ by $a_{L,d}$.

As a was obtained from the measurement, the estimate of k_La requires only the estimation of k_L. As mentioned above, the mass transfer coefficient, k_L was reported as a function of liquid properties and bubble size. It was assumed that Schmidt number remained constant as salinity did not significantly alter the properties of the liquid [15,31–33], and hence, the dimensionless relationship between Sherwood number (Sh), Reynold number (Re), Schmidt number (Sc) and Grashof number (Gr) could be formulated as follows:

forced convection

$$Sh = a + \underbrace{bGr^c Sc^d}_{\text{free convection}} + \underbrace{e\ Re^f\ Sc^h}_{\text{forced convection}} \quad (14)$$

Generally, Grashof number, Gr, represents the mass transfer by natural convection or free rise velocity whilst Reynolds number, Re, is the mass transfer form forced convection:

$$Gr = \frac{d_{Bs}^3 \rho_l \Delta\rho g}{\mu_l^2} \quad (15)$$

$$Re = \frac{d_{Bs} v_s \rho_l}{\mu_l} \quad (16)$$

The velocity and bubble diameter used in the calculation of Reynolds number were the slip velocity, v_s, and Sauter mean diameter, d_{Bs}. The slip velocity in riser, $v_{s,r}$ was calculated as a function of the terminal rise velocity of a single bubble, u_∞, which were related to hindering effects from neighboring bubbles in the riser section. Information on bubble sizes was then employed to estimate the slip velocity of the gas bubbles in the system using the following equation [34,35]:

$$v_{s,r} = \frac{u_\infty}{(1 - \varepsilon_{g,r})} \quad (17)$$

where u_∞ is the terminal bubble riser velocity which can be calculated using the correlation proposed by Jamialahmadi et al. [36].

$$u_\infty = \frac{(1/8)((\rho_l - \rho_g)/\mu_l) g d_{Bs}^2 ((3\mu_l + 3\mu_g)/(2\mu_l + 3\mu_g)) \sqrt{2\sigma/d_{Bs}(\rho_l + \rho_g) + g d_{Bs}/2}}{\sqrt{[(1/8)((\rho_l - \rho_g)/\mu_l) g d_{Bs}^2 ((3\mu_l + 3\mu_g)/(2\mu_l + 3\mu_g))]^2 + 2\sigma/d_{Bs}(\rho_l + \rho_g) + g d_{Bs}/2}} \quad (18)$$

The parameters a–h in Eq. (14) was then determined from experiments.

Eq. (14) must be used to predict $k_{L,r}$ and $k_{L,d}$, and in doing so, the slip velocities or terminal rise velocities in both riser and downcomer must be known (from Eqs. (17) and (18)) for the calculation of Reynolds number. As the photographic technique could only be used to measure the bubble size in riser, bubble size in downcomer was not known and the determination of slip velocity in downcomer was not possible. However, the average bubble size in downcomer ($d_{B,d}$) could be estimated from the

Table 7
Parameter estimates for correlation in Eq. (14) $Sh = a + bGr^c Sc^d + eRe^f Sc^h$

Salinity (ppt)	Parameter							R^2
	a	*b*	*c*	*d*	*e*	*f*	*h*	
0	0.41	1.05	048	0	0	0	0	0.91
15–45	0.41	1.04	0.16	0.3	0.13	0.46	0.06	0.81
0 [4]	0.5	1.07	0.47	0	0	0	0	0.92

downcomer liquid velocity, $u_{L,d}$, by assuming that the liquid must have velocity equaled to the terminal velocity to be able to drag the bubble down into the downcomer, or

$$v_{s,d} = u_{L,d} \tag{19}$$

Once the terminal velocity was known, the Levich equation [37] as shown in Eq. (19) was proposed for the calculation of bubble size:

$$d_{B,d} = \frac{1.8}{g}\left(\frac{u_{L,d}}{2}\right)^2 \tag{20}$$

Assume that there was no variation of bubble size along the radial and axial directions in downcomer:

$$d_{Bs,d} = d_{B,d} \tag{21}$$

The $a_{L,d}$ was calculated from substitution of $d_{Bs,d}$ from Eq. (21) and $\varepsilon_{g,d}$ from the experiment to Eq. (4).

The parameters *a–h* in Eq. (14) were evaluated using non-linear parameter fittings using all the results available in this work, and the results are given in Table 7 (noted that these parameters were obtained from the solver function in the MS Excel 97 where the objective was a minimal error between experimental and simulation data). For the case of tap water, the results from parameter fitting were reasonably close to those proposed from Wongsuchoto et al. [4] (as shown in the last row of Table 7). The fittings for the saline water gave somewhat different results from that for pure water in that the terms Reynolds number was not involved in the pure water system, but it was, to certain extent, for the saline water systems. This meant that the mechanism controlling the mass transfer coefficient in pure water was only the natural convection whereas the force convection as represented by the Reynolds term also was significant in the system operated with saline water. Fig. 11 illustrates the comparison between the calculated and experimental k_La of the airlift contactor operated with various saline solutions.

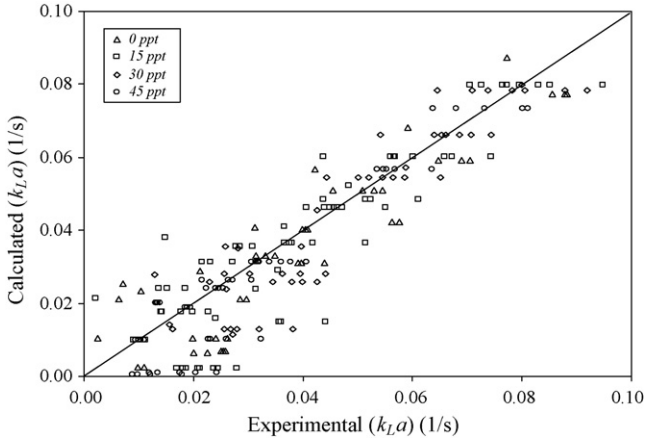

Fig. 11. Comparison of k_La from experiment and k_La estimated by Eq. (14) in ALC (A_d/A_r = 0.067–0.661).

4. Conclusion

This work continued our previous work on the bubble size distribution in the airlift systems. The distribution of bubble size in saline solution which was often used in cell cultivation was provided. Mechanisms for the bubble breakup/coalescence were proposed. The relationship between bubble size, liquid properties and the gas–liquid mass transfer behavior was investigated where the correlation for the estimate of the overall volumetric mass transfer coefficient was proposed with reasonable accuracy. This information will be useful in the future design of the airlift reactors for specific applications.

Acknowledgements

The authors wish to acknowledge the Thailand Research Fund and the Graduated Research Fund at Chulalongkorn University, THAILAND, for their financial supports.

References

[1] M.Y. Chisti, Airlift Bioreactors, Elsevier Applied Science, London/New York, 1989.
[2] D. Colella, D. Vinci, R. Bagatin, M. Masi, E.A. Bakr, A study on coalescence and breakage mechanisms in three different bubble columns, Chem. Eng. Sci. 54 (1999) 4767–4777.
[3] M. Polli, M.D. Stanislao, R. Bagatin, E.A. Bakr, M. Masi, Bubble size distribution in the sparger region of bubble columns, Chem. Eng. Sci. 57 (2002) 197–205.
[4] P. Wongsuchoto, T. Charinpanitkul, P. Pavasant, Bubble size distribution and gas–liquid mass transfer in airlift contactors, Chem. Eng. J. 92 (2003) 81–90.
[5] K. Kaewpintong, A. Shotipruk, S. Powtongsuk, P. Pavasant, Photoautotrophic high-density cultivation of *Haematococcus pluvialis* in airlift bioreactor, Bioresour. Technol. 98 (2007) 288–295.
[6] S. Krichnavaruk, W. Loataweesup, S. Powtongsook, P. Pavasant, Optimal growth conditions and the cultivation of *Chaetoceros calcitrans* in airlift photobioreactor, Chem. Eng. J. 10 (2005) 91–98.
[7] S. Krichnavaruk, S. Powtongsook, P. Pavasant, Enhanced productivity of *Chaetoceros calcitrans* in airlift photobioreactors, Bioresour. Technol. 98 (2007) 2123–2130.
[8] J. Bo, P. Lant, Flow regime, hydrodynamics, floc size distribution and sludge Properties in activated sludge bubble column, air-lift and aerated stirred reactors, Chem. Eng. Sci. 59 (2004) 2379–2388.

[9] N. Kantarci, F. Borak, O.K. Ulgen, Bubble column reactors, review, Process Biochem. 40 (2005) 2263–2283.
[10] M. Bouaifi, G. Hebrard, D. Bastoul, M. Roustan, A comparative study of gas holdup, bubble size, interfacial area and mass transfer coefficients in stirred gas–liquid reactors and bubble columns, Chem. Eng. Proc. 40 (2001) 97–111.
[11] J.C. Merchuk, A. Contreras, F. Garcia, E. Molina, Studies of mixing in a concentric tube airlift bioreactor with different spargers, Chem. Eng. Sci. 53 (1998) 709–719.
[12] L. Guo-Qing, Y. Shou-Zhi, C. Zhao-Ling, C. Jia-Yong, Mass transfer and gas–liquid circulation in an airlift bioreactor with viscous non-newtonian fluid, Chem. Eng. J. The Biochem. Eng. J. 56 (1995) B101–B107.
[13] J.M.T. Vasconcelos, J.M.L. Rodrigues, S.C.P. Orvalho, S.S. Alves, S.R.L. Mendes, A. Reis, Effect of contaminants on mass transfer coefficients in bubble column and airlift contactors, Chem. Eng. Sci. 58 (2003) 1431–1440.
[14] W.A. Al-Masry, Effects of antifoam and scale-up on operation of bioreactors, Chem. Eng. Processing 38 (1999) 197–201.
[15] P. Painmanakul, K. Loubére, G. Hebrard, M. Mietton-Peuchot, M. Roustan, Effect of surfactants on liquid-side mass transfer coefficients, Chem. Eng. Sci. 60 (2005) 6480–6491.
[16] G. Hebrard, D. Bastoul, M. Roustan, Influence of the gas sparger on the hydrodynamic behavior of bubble columns, Trans. Inst. Chem. Eng. 74 (1996) 406–414.
[17] A. Couvert, M. Roustan, P. Chatellier, Two-phase hydrodynamic study of a rectangular airlift loop reactor with an internal baffle, Chem. Eng. Sci. 54 (1999) 5245–5252.
[18] M.Y. Chisti, M. Moo-Young, Hydrodynamics and oxygen mass transfer in a pneumatic bioreactor devices, Biotechnol. Bioeng. 31 (1988) 487–494.
[19] K. Koide, H. Sato, S. Iwamoto, Gas holdup and volumetric liquid-phase mass transfer coefficient in bubble column with draught tube and with gas dispersion into annulus, J. Chem. Eng. Jpn. 16 (5) (1983) 407–413.
[20] R.R. Lessard, A.S. Zieminiski, Bubble coalescence and gas transfer in aqueous electrolytic solutions, Ind. Eng. Chem. Fundam. 10 (1971) 260–269.
[21] G. Marrucci, A theory of coalescence, Chem. Eng. Sci. 24 (1969) 975–985.
[22] M.J. Prince, H.W. Blanch, Transition electrolyte concentrations for bubble coalescence, AIChE J. 36 (1990) 1425–1429.
[23] G. Marrucci, L. Nicodemo, Coalescence of gas bubbles in aqueous solution of inorganic electrolytes, Chem. Eng. Sci. 22 (1967) 1257–1265.
[24] M.J. Prince, H.W. Blanch, Bubble coalescence and breakup in air-sparged bubble column, AIChE J. 36 (1990) 1485–1499.
[25] P.K. Weissenborn, R.J. Pugh, Surface tension of aqueous solutions of electrolytes: relationship with ion hydration, oxygen solubility, and bubble coalescence, J. Colloid Interface Sci. 184 (1996) 550–563.
[26] K. Malysa, M. Krasowska, M. Krzan, Influence of surface active substances on bubble motion and collision with various interfaces, Adv. Colloid Interface Sci. 114–115 (2005) 205–225.
[27] Y.H. Tsang, K. Young-Ho, L.K. Donald, Bubble-size dependence of the critical electrolyte concentration for inhibition of coalescence, J. Colloid Interface Sci. 275 (2004) 290–297.
[28] W.F. Cain, C.J. Lee, A technique for studying the drainage and rupture of unstable liquid films formed between two captive bubbles: Measurements on KCl solutions, J. Colloid Interface Sci. 106 (1985) 70–85.
[29] S. Hartland, Surface and Interface Tension: Measurement, Theory, and Applications Basel:, Marcel Dekker, New York, 2004.
[30] A. Contreras, F. Garcia, E. Molina, J.C. Merchuk, Influence of sparger on energy dissipation, shear rate, and mass transfer to sea water in a concentric-tube airlift bioreactor, Enzyme Microb. Technol. 25 (1999) 820–830.
[31] R. Higbie, Rate of absorption of a pure gas into a still liquid during short period of exposure, Trans. Am. Inst. Chem. Eng. 31 (1935) 365–389.
[32] P.H. Calderbank, Mass transfer in fermentation equipment, in: N. Blakebrough (Ed.), Biochemical and Biological Engineering Science, vol. 2, Academic Press, New York, 1967.
[33] J.E. Bailey, D.F. Ollis, Biochemical Engineering Fundamentals, McGraw-Hill, New York, 1977.
[34] G. Marrucci, Rising velocity of a swarm of spherical bubbles, Ind. Eng. Chem. Fundam. 4 (1965) 224–225.
[35] G.B. Wallis, One Dimensional Two-Phase Flow, McGraw-Hill, New York, 1969.
[36] M. Jamialahmadi, C. Branch, Müller-Steinhagen, Terminal bubble rise velocity in liquid, Trans. Inst. Chem. Eng. Part A 72 (1994) 119–122.
[37] V.G. Levich, Physiochemical Hydrodynamis, Prentice-Hall, Englewood Cliffs, NJ, 1962.